



Rainbow trapping based on higher-order topological corner modes: supplement

LI LIANG,^{1,†} XIAOXI ZHOU,^{2,†} JUN-HUI HU,¹  HAI-XIAO WANG,^{1,3}  JIAN-HUA JIANG,² AND BO HOU^{2,4}

¹*School of Physical Science and Technology, Guangxi Normal University, Guilin 541004, China*

²*School of Physical Science and Technology & Collaborative Innovation Center of Suzhou Nano Science and Technology, Soochow University, Suzhou 215006, China*

³*e-mail: hxwang@gxnu.edu.cn*

⁴*e-mail: houbo@suda.edu.cn*

[†]*These authors contributed equally.*

This supplement published with Optica Publishing Group on 10 March 2022 by The Authors under the terms of the [Creative Commons Attribution 4.0 License](https://creativecommons.org/licenses/by/4.0/) in the format provided by the authors and unedited. Further distribution of this work must maintain attribution to the author(s) and the published article's title, journal citation, and DOI.

Supplement DOI: <https://doi.org/10.6084/m9.figshare.19115540>

Parent Article DOI: <https://doi.org/10.1364/OL.451770>

Supplementary Material for

Rainbow trapping based on higher-order topological corner modes

Li Liang¹, Xiaoxi Zhou², Jun-Hui Hu¹, Hai-Xiao Wang^{1*}, Jian-Hua Jiang^{2,*}, and Bo Hou^{2*}

¹School of Physical Science and Technology, Guangxi Normal University, Guilin 541004, China

²School of Physical Science and Technology & Collaborative Innovation Center of Suzhou Nano Science and Technology, Soochow University, Suzhou 215006, China

* Author to whom correspondence should be addressed: hxwang@gxnu.edu.cn (H.- X. Wang), jianhuajiang@suda.edu.cn (J. -H. Jiang), houbao@suda.edu.cn (B. Hou)

(I) High-order topology characterization via crystalline symmetry

In this part, we present the details of symmetry representations at the high symmetric points (HSPs) in the Brillouin zone (BZ), which are utilized to characterize the higher-order topology. It is known that the topological crystalline index can be expressed by the full set of the C_3 eigenvalues at the high-symmetry points (HSPs) [1]. For an HSP denoted by the symbol Π , the C_3 eigenvalues can only be $\Pi_n = e^{i2\pi(n-1)/3}$ with $n = 1, 2, 3$. Here, the HSPs include the Γ , K and K' points. The full set of C_3 eigenvalues at the HSPs are redundant due to the time-reversal symmetry and the conservation of the number of bands below the band gap. The minimal set of indices that describe the band topology is given by

$$[K]_n = \#K_n - \#\Gamma_n \quad (1)$$

where $\#K_n(\#\Gamma_n)$ is the number of bands below the band gap with symmetry eigenvalue $K_n(\Gamma_n)$ at the $K(\Gamma)$ points. In this scheme, the point Γ is taken as the reference point to get rid of the redundancy. For the trivial atomic insulator (i.e., the band gap formed by uncoupled atoms), all the HSPs have exactly the same symmetry eigenvalues. Therefore, the trivial atomic insulators have $[\Pi]_n$ for all the HSP. In contrast, any nonzero $[\Pi]_n$ indicates a topological band gap that is adiabatically disconnected from the trivial atomic insulator.

In our cases, the topological indices can be written in a compact form as $\chi = ([K_1], [K_2])$. To obtain the C_3 eigenvalues at $K(\Gamma)$ points, we display the phase field patterns of various breathing kagome PhCs in Fig. S1. It is evident that the C_3 eigenvalues at $K(\Gamma)$ points for BK1 and BK2 are 1, indicating that both BK1 and BK2 are trivial phases. For BK3 (BK4), the C_3 eigenvalue at Γ point is 1(1), while at K point is $e^{\frac{i2\pi}{3}}$ ($e^{\frac{i4\pi}{3}}$), indicating that both BK3 and BK4 are nontrivial phases.

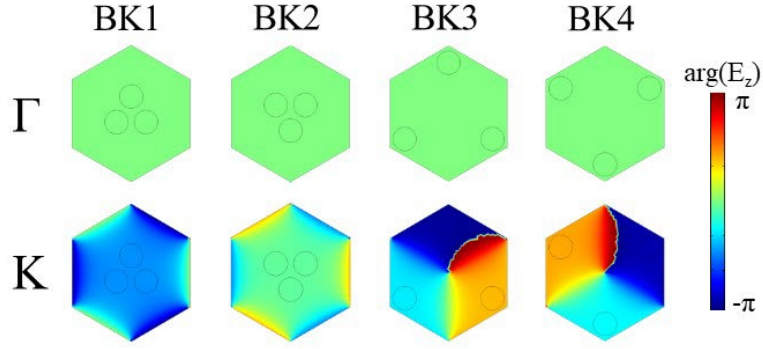


Figure S1 The phase patterns of electric field at HSPs, which give C_3 symmetry eigenvalues.

Therefore, the topological indice is $\chi_1 = (0,0)$ for both BK1 and BK2, $\chi_2 = (-1,1)$ for BK3, and $\chi_3 = (-1,0)$ for BK4. We list the topological index of the breathing kagome PhCs in Table I.

Table I The topological index of the breathing kagome PhCs.

	Invariants		χ
	$[K_1^3]$	$[K_2^3]$	
BK1	0	0	$\chi_1=(0,0)$
BK2	0	0	$\chi_1=(0,0)$
BK3	-1	1	$\chi_2=(-1,1)$
BK4	-1	0	$\chi_3=(-1,0)$

(II) Tight-binding models on triangular-shaped supercells

For 2D photonic breathing kagome lattice, the higher-order bulk-edge correspondence does not tell the exact number of the HOTCMs. In fact, the number of HOTCMs depends on the geometric configurations of the corners. To this end, we construct tight-binding models on triangular-shaped supercells.

We first study the tight-binding model with next-nearest neighbor hopping on the T_A and T_B , where the outer claddings are trivial PhCs. For convenience, we ignore the outer cladding structure and only consider the inner structure with nontrivial

topological phase. As displayed in Fig. S2(a), the bulk (edge) of the T_A consists of trimers (isolated dimers), while the corner (colored in red) consists of an isolated site. By solving the tight-binding Hamiltonian of the finite systems, we present the eigen energy solutions in Fig. S2(b). It is observed that three degenerate states (colored in red) are pinned to zero-energy level owing to the generalized chiral symmetry [2], namely type-I HOTCMs, while other three degenerate states (colored in blue) follow closely the spectrum of the topological edge states [3], namely type-II HOTCMs. Moreover, the type-I and type-II HOTCMs also make a difference on their eigen modes, as depicted in Fig. S2(c). In a similar way, we construct another tight-binding model on the T_B . The geometric configuration of the corner of the T_B in Fig. S2(d) shows that there exist two isolated sites, which may result in different HOTCMs. As expected, the eigen spectrum consists of two sets of type-I HOTCMs with different frequencies as well as a set of type-II HOTCMs in the band gap, which successfully explain our simulation results in Fig. 2(e).

We then proceed to consider the tight-binding model on the T_C and T_D . As shown in Fig. S2(g), the corner area between the inner and outer structures of the T_C only consists of one lattice site (colored in red). The eigen solution of the tight-binding of the T_C presented in Fig. S2(h) shows that there are six HOTCMs, including both type-I and type-II, of which the eigen modes are presented in Fig. S2(i). It is worthy to point out that the HOTCMs in the band gap owing to the outer structure with nontrivial topological phase are also observed. By exchanging the outer and inner structure of the T_C , we have another tight-binding model T_D , as depicted in Fig. S2(j). Note that the corner area between the inner and outer structures of T_D consists of two lattice sites, and the eigen solutions as well as the eigen states of HOTCMs in Fig. S2(k) and S2(l) make a difference with other tight-binding modes.

To sum up, our simulation results of the HOTCMs in various triangular-shaped supercell in Fig. 2 can be successfully explained via the tight-binding approach.

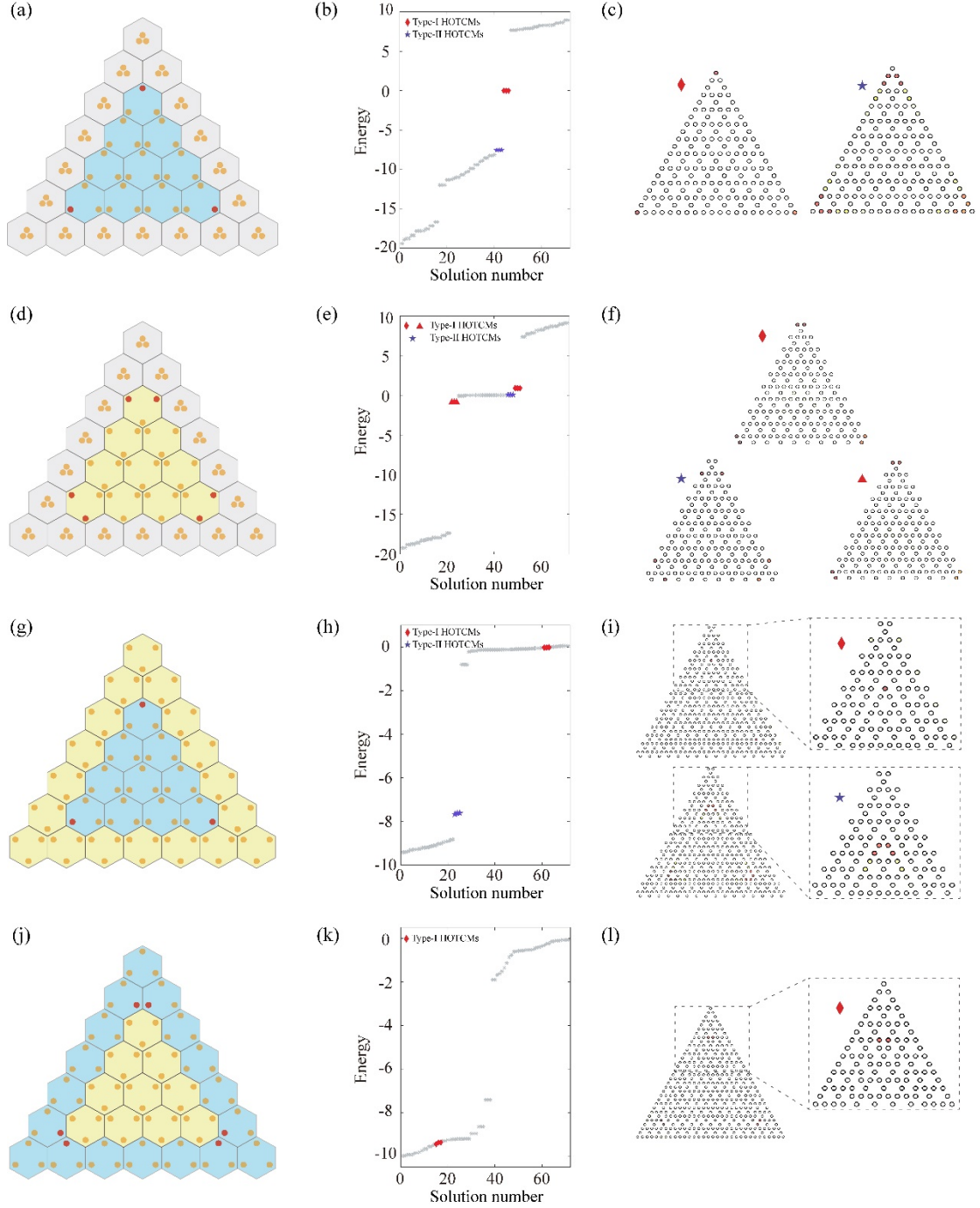


Figure S2 (a,d,g,j) Schematic of the tight-binding models on triangular-shaped supercell formed by (a) the BK3 (inner) and the BK1 (outer), which belong to phase χ_2 and χ_1 , respectively, (d) the BK4 (inner) and the BK1 (outer), which belong to phase χ_3 and χ_1 , respectively, (g) the BK3 (inner) and the BK4 (outer), which belong to phase χ_2 and χ_3 , respectively, (j) the BK4 (inner) and the BK3 (outer), which belong to phase χ_3 and χ_2 , respectively. (b,e,h,k) Eigen solution of the tight-binding model on the (b) T_A, (e) T_B, (h) T_C, (k) T_D. Note that the different corner configurations

are highlighted by colored dot. The corresponding eigen states of type-I and type-II HOTCMs in the tight-binding models are also displayed in order in (c,f,i,l).

(III) Tight-binding models on hexagon-shaped supercells

Following above, we continue to construct tight-binding models on hexagon-shaped supercell as we have studied in Fig. 3. We first study the tight-binding model with next-nearest neighbor hopping on the H_A , which the outer claddings are trivial PhCs. For convenience, we ignore the outer cladding structures and only consider the inner structures with nontrivial topological phase. As shown in Fig. S3(a), the supercell consists of trimers in the bulk and is featured by armchair-type boundary. Specifically, thanks to the symmetry constrain, there exist two types of corner geometric configuration, one consisting of an isolated site and the other consisting of two isolated sites. The former is distributed in up-triangular array while the latter are distributed in down-triangular array. As a result, the number of HOTCMs shall be more than that in the triangular-shaped supercell [see Fig. S3(b) and 3(c)]. It is seen that there exists two HOTCMs localized at down-triangular distributed corners with higher energy, while three HOTCMs localized at up-triangular distributed corners. By inspecting their eigen states in the tight-binding model of the H_A in Fig.S3(c), we find that there is a fundamental difference between type-I and type-II HOTCMs, which originate from nearest- and next-nearest- neighboring coupling, respectively.

In a similar way, we proceed to study the tight-binding model on the H_B , as depicted in Fig. S3(d). It is seen that the supercell consists of trimers in the bulk and is featured by armchair-type boundary. Although there still exist two corner geometric configurations (one isolated site and two isolated sites), the one isolated site corners are inside the supercell, whereas the two isolated site corners are outside the supercell, leading to distinct energy spectrum [see Fig. S3(e)]. By inspecting the eigen states of the HOTCMs in Fig. S3(f), we find that there exist two type-I and type-II HOTCMs.

In summary, the tight-binding models on hexagon-shaped supercells give the main features of HOTCMs in Fig. 3, which explain the origin of the HOTCMs.

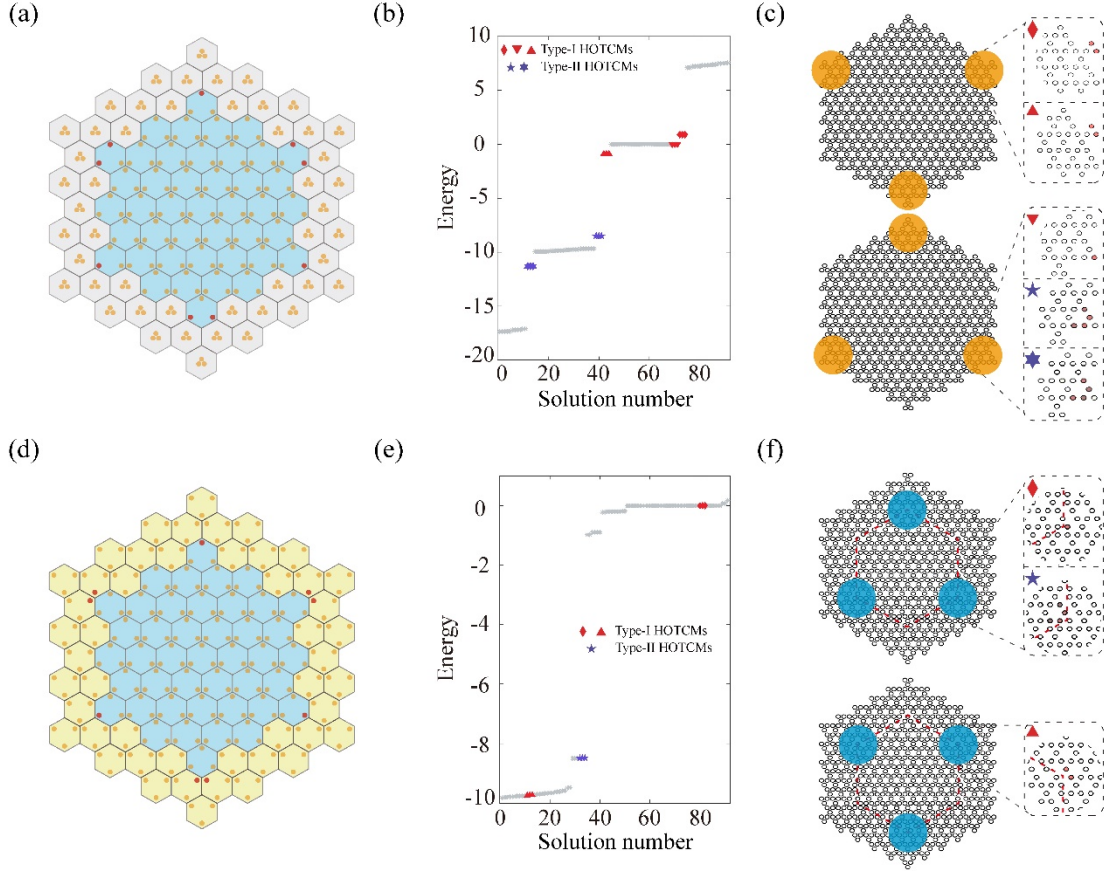


Figure S3 (a,d) Schematic of the tight-binding models on hexagon-shaped supercell formed by (a) the BK3 (inner) and the BK1 (outer), which belong to phase χ_2 and χ_1 , respectively, (d) the BK3 (inner) and the BK4 (outer), which belong to phase χ_2 and χ_3 , respectively. (b,e) Eigen solutions of the tight-binding model on the (b) H_A and (e) H_B . Note that the corner states are highlighted by colored dot. The corresponding field patterns of type- I and type-II HOTCMs are also displayed in order in (c,f).

(IV) The analysis on the polygon structure with multiple configurations of corners

To verify the rainbow trapping effect, we propose a polygon structure where inner and outer PhCs belong to distinct topological phases in the maintext. Such a structure containing seven corners with intersection angles of $60^\circ, 120^\circ, 150^\circ$ and 240° . Specifically, we have demonstrated that those corners with intersection angles of 60° and 120° , labeled as C1, C2, C3 and C4, can support HOTCMs in Figs. 2 and 3. Here we further discuss the other three corners by calculating their eigen solutions.

To check whether HOTCMs survive in the corner with intersection angles of 150° ,

we construct a regular dodecagon-shaped supercell, where the BK3 is surrounded by the BK1 [see the inset of Fig.S4 (a)]. From the eigen spectrum depicted in Fig. 4(a), it is evident that there is no HOTCMs except the bulk and edge states, indicating that the corner with intersection angle of 150° does not support the HOTCM. In addition, we also design a rhombus-shaped structure that containing corners with 240° and 300° , where BK1 is embedded in BK3 [see the inset of Fig. S4(b)]. By inspecting the eigen spectrum and corresponding eigen modes in Fig. S4, we find that there is no HOTCMs emerging in the corners with 240° except a type-I HOTCM localized at the corner with 300° [see the field pattern of HOTCM in the inset of Fig. S4(b)]. Therefore, we theoretically demonstrate that only the intersection angles of 60° and 120° , labeled as C1, C2, C3, and C4 in the polygon structure, can support HOTCMs.

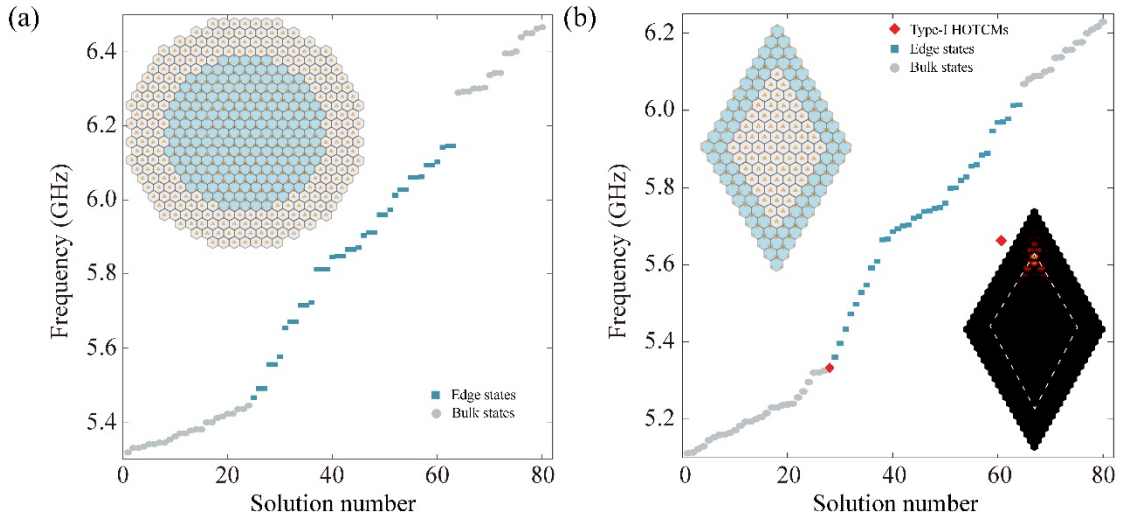


Figure S4 Eigen spectrum of (a) dodecagon-shaped supercell consisting of the BK1 and the BK3. Inset: schematic of dodecagon-shaped supercell. (b) Rhombus-shaped structure supercell consists of the BK1 and the BK3. Inset: schematic of rhombus-shaped structure and the eigen mode of HOTCMs localized at the corner with intersection angle of 60° .

V. Rainbow trapping with well-localized HOTCMs

In the main text, we theoretically and experimentally demonstrate the rainbow trapping effect in a well-designed polygon-shaped structure. However, due to the low

primitivity of the dielectric rods ($\varepsilon = 4.8$) and narrow band gap, the excited HOTCMs are not localized well. To this end, we improve the rainbow trapping effect by optimizing the PhCs with higher primitivity of the dielectric rods ($\varepsilon = 7$). Other parameters of the optimal PhCs are listed as follows: the radius of the dielectric rod $r = 0.15a$ and the lattice constant $a = 10mm$.

As shown in Fig. S5(a), the polygon-shaped structure R1 consists of the BK3 and the BK1, where the BK3 is embedded in the BK1. Note that those corners supported HOTCMs are labeled. The whole structure is surrounded by perfect match layers (PMLs) to avoid unwanted scattering. The eigen spectrum displayed in the left panel of Fig. S5(b) shows that there exist some modes in the band gap, indicating well-localized HOTCMs. To excite the HOTCMs, we place the point source (indicated by the pentacle) around the C1 as well as the detecting probes around C1, C2, C3, and C4, respectively. By scanning the frequency of point source from 8GHz to 10 GHz with step of 0.05GHz, we obtain the transmission spectra for C1, C2, C3, and C4, as depicted in the right panel of Fig. S5(b). It is seen that the transmission for C4 is very weak, which is attributed to the nonlocal eigen mode. To check whether the rainbow trapping still survives, we also present the excited electric field profiles of HOTCMs in Fig. S5(c). As expected, HOTCMs are excited in anticlockwise corner order, i.e., $C1 \rightarrow C2 \rightarrow C3 \rightarrow C4 \rightarrow C1$, indicating the rainbow trapping effect. Moreover, the HOTCMs look more localized in comparison to that in Fig. 4(d) with low permittivity of the dielectric rods.

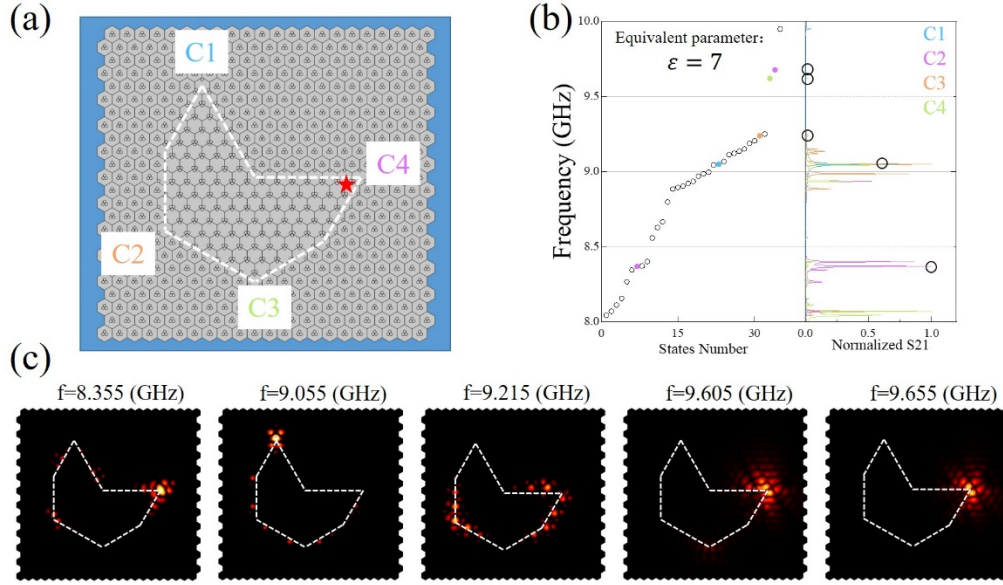


Figure S5 (a) Schematic of the polygon structure R1 made of the BK3 (inner) and BK1 (outer). Four corners are labeled as C1, C2, C3 and C4. A point source is placed around C4. The adopted boundary is the perfect match layer. (b) Left panel: the eigen spectrum of the R2. Right panel: The transmission spectra for C1 (blue), C2 (orange), C3 (green) and C4 (purple). (c) The excited field patterns of five HOTCMs in anticlockwise corner order with raising frequency, i.e., $C4 \rightarrow C1 \rightarrow C2 \rightarrow C3 \rightarrow C4$. The white lines refer to the boundary of the polygon.

In addition, we study another polygon-shaped structure R2, as depicted in Fig. S6(a). The other parameters are same as that in Fig. S5(a). To see whether the rainbow trapping effect persists, we display the eigen spectrum of the R2 in the left panel of Fig. S6(b). At this time, the HOTCMs with maximal and minimal frequencies are localized at C1 while the other three are localized at C2, C3, and C4 in a lowering frequency order. We measure transmission spectra of C1, C2, C3, and C4 by placing a point source around C3 [see the inset in Fig. S6(a)] and the detecting probes at C1, C2, C3, and C4, respectively. The measured spectra of HOTCMs are displayed in the right panel of Fig. S6(b). It is seen that the HOTCMs are excited in a clockwise corner order, i.e., $C1 \rightarrow C4 \rightarrow C3 \rightarrow C2 \rightarrow C1$, indicating the rainbow trapping effect in R2. Specifically, the HOTCMs look more localized in comparison to that in Fig. 5(d) with low permittivity

of the dielectric rods.

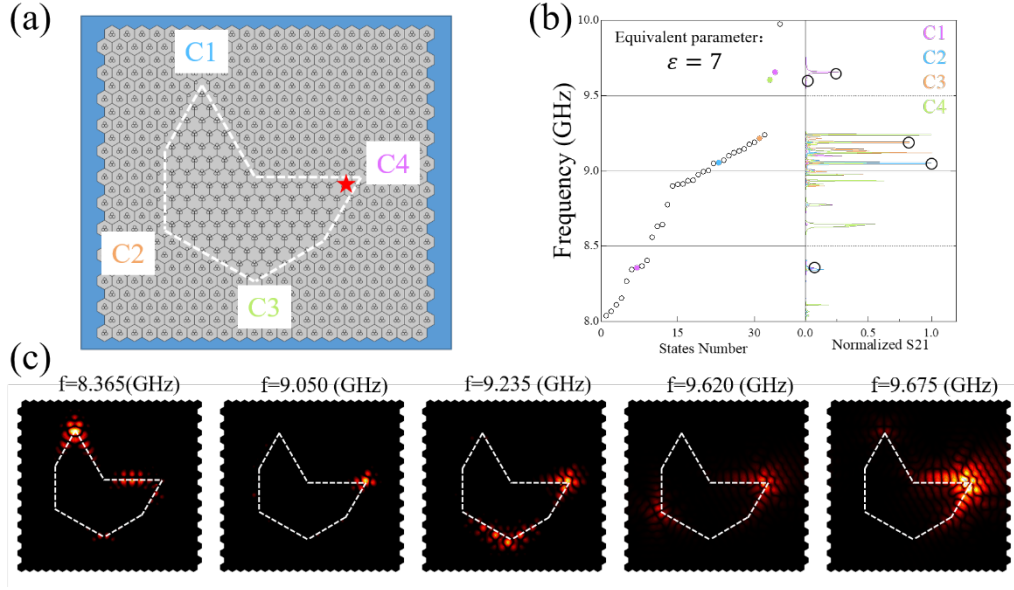


Figure S6 (a) Schematic of the polygon structure R2 made of the BK4 (inner) and the BK1 (outer). Four corners are labeled as C1, C2, C3, and C4. A point source is placed around C4. The adopted boundary is the perfect match layer. (b) Left panel: the eigen spectrum of the R2. Right panel: The transmission spectra for C1 (blue), C2 (orange), C3 (green) and C4 (purple). (c) The excited field patterns of five HOTCMs in clockwise corner order with raising frequency, i.e., $C1 \rightarrow C4 \rightarrow C3 \rightarrow C2 \rightarrow C1$. The white lines refer to the boundary of the polygon.

Reference:

- [1] W. A. Beanalcazar, T. Li, T. L. Hughes, Quantization of fractional corner charge in C_n -symmetric higher-order topological crystalline insulators, *Phys. Rev. B* **2019**, *99*, 245151.
- [2] Xiang Ni, M. Weiner, A. Alù, A. B. Khanikaev, Observation of higher-order topological acoustic states protected by generalized chiral symmetry, *Nat. Mat.* **2019**, *18*, 113.
- [15] M. Li, et al., Higher-order topological states in photonic kagome crystals with long-range interactions, *Nat. Photon.* **2020**, *14*, 89.
- [16] H.-X. Wang, L. Liang, B. Jiang, J. Hu, X. Lu, J.-H. Jiang, Higher-order topological phases in tunable C_3 symmetric photonic crystals. *Photon. Res.* **2021**, *9*, 1854.